Published in final edited form as:
J Phys Chem C Nanomater Interfaces. 2011 June 9; 115(22): 11030–11035. doi:10.1021/jp2032302.

Sintering Rate and Mechanism of TiO_2 Nanoparticles by Molecular Dynamics

B. Buesser, **A.J. Gröhn**, and **S.E. Pratsinis***
Particle Technology Laboratory, Institute of Process Engineering, Department of Mechanical and Process Engineering, ETH Zurich, 8092 Zürich, Switzerland

Abstract

Titania is the dominant white pigment and photocatalytic material, a key component of sunscreens and has promising applications in photovoltaics and sensors of organic vapors. The growth of TiO_2 nanoparticles by sintering, the critical step during their large scale manufacture and processing, is elucidated and quantified by molecular dynamics. Highly mobile ions from the particle surface fill in the initially concave space between nanoparticles (surface diffusion) forming the final, fully-coalesced, spherical-like particle with minimal displacement of inner Ti and O ions (grain boundary diffusion) revealing also the significance and sequence of these two sintering mechanisms of TiO_2. A sintering rate for TiO_2 nanoparticles is extracted that is much faster than that in the literature but nicely converges to it for increasing particle size.

Keywords

nanotechnology; aerosol science; solid state; surface diffusion

1. Introduction

Titania (TiO_2) nanoparticles have many attractive applications in photovoltaic[1] and photocatalytic[2] processes as well as chemo-resistive gas sensors[3] and sunscreens[4], while possible health effects of these nanoparticles are investigated[5]. The performance of TiO_2 nanoparticles depends considerably on their size and composition which are determined by their sintering rate during synthesis and/or post-processing. The sintering rate determines the growth rate of nanoparticles and is crucial for design of their gas-phase synthesis with controlled size, structure, composition and eventual performance in a number of applications[6].

Most studies of sintering during synthesis of nanoparticles extract effective rather than intrinsic sintering rates of TiO_2[7-11]. In contrast, Seto *et al.*[12] have proposed a sintering rate for TiO_2 and validated it by accounting for the detailed fluid mechanics of their hot wall reactor forming rather large TiO_2 nanoparticles (d_p = 10 – 100 nm). Little is known, however, for the sintering rate of small TiO_2 nanoparticles (d_p < 10 nm) as it is difficult to reliably measure it.

On the other hand molecular dynamics (MD) simulations have been used to study the sintering to full coalescence of metallic and metalloid nanoparticles[13,14] though much less

*Corresponding author: +41-44-632-3180; fax: -1595; pratsinis@ptl.mavt.ethz.ch.

Supporting Information Available: Surface area evolution for different initial particle orientations for $d_{p,0}$ = 3 nm and T = 1800 K. Surface area evolution for $d_{p,0}$ = 2.5 nm and T = 1500 – 1800 K. This material is available free of charge via the internet at http://pubs.acs.org.

Europe PMC Funders Author Manuscripts

has been done for ceramic ones as their force fields and potentials are difficult to determine. Nevertheless Collins *et al.*[15] identified three stages of TiO_2 sintering (contact, locking and fusion) using the force field of Matsui and Akaogi[16]. Similarly, Koparde and Cummings[17] investigated the sintering of two TiO_2 nanoparticles up to $t = 0.5$ ns by tracking the shrinkage of the center-to-center distance and the growth of the sintering neck. They compared MD with phenomenological sintering models, investigated the melting of TiO_2 nanoparticles[18] and found that the transformation size of anatase to rutile titania was only 1.65 nm at $T = 1473$ K which was further decreased for increasing T[19].

The above MD simulations for TiO_2 sintering have reached up to no more than 1 ns residence time, a duration that is not sufficient for complete coalescence of the considered particles. So most of the surface area reduction of such small particles has taken place by adhesion (contact) and neck growth (locking) that limited the detailed understanding of sintering mechanisms and, most importantly, the extraction of quantitative sintering rates that are needed in systematic process design for manufacturing nanoparticles.

Here, the complete sintering of rutile TiO_2 nanoparticles is investigated by accelerated MD[20] from adhesion and neck growth to finally full coalescence up to several hundred nanoseconds. This allows determining the sintering rate of very small TiO_2 nanoparticles ($d_p < 5$ nm) by monitoring the evolution of their surface area and comparing it to that of larger particles[12,21]. Here the sintering mechanism of TiO_2 is unraveled and its rate of sintering or coalescence is quantified, bridging the gap of knowledge from a few molecules to several nanometers, the key size range for nanoparticle properties and performance.

2. Theory

2.1 Molecular Dynamics

The Buckingham-type potential, U, of Matsui and Akaogi[16] is used here as it reproduces best the TiO_2 crystal structures of rutile, anatase and brookite[22]:

$$U\left(r_{ij}\right) = A_{ij}\exp\left(-\frac{r_{ij}}{B_{ij}}\right) - \frac{C_{ij}}{r_{ij}^6} + k\frac{q_i q_j}{r_{ij}} \quad (1)$$

where r_{ij} is the distance between the centers of ions i and j with their charges q_i and q_j, respectively. The constants A_{ij}, B_{ij} and C_{ij} depend on the Ti or O ion combination. The performance of this force field was investigated for simulation of the (110) surface of rutile TiO_2 and, even though it was developed for bulk TiO_2, quite good agreement was found in terms of bond lengths[23]. This potential also gives similar results to computationally more demanding polarizable force fields[24]. Comparison of the above force field with density functional theory (DFT) showed good agreement for clusters larger than Ti_9O_{18}[25].

Here, charge neutral, spherical particles with diameter $d_{p,0} = 2 - 4$ nm have been cut out from a perfect rutile TiO_2 crystal made of multiples of its unit cell[26]. These particles were equilibrated by temperature rescaling for 100 ps with a timestep of 1 fs[22]. The quality of equilibration and energy conservation has been tested by integration in the microcanonical ensemble (NVE) for additional 100 ps. Two particles with different initial ion velocity distribution at each temperature and diameter have been prepared. These have been combined to one simulation with a minimum separation of 0.3 nm between the closest ion centers of the two particles. For each diameter and temperature, four simulations were carried out by initially turning the second particle by 0, 90, 180 and 270°. Sintering simulations have been carried out in the microcanonical (NVE, constant energy) and NVE combined with velocity scaling every 10^3 timesteps of 1 or 3 fs[22] (conserved temperature) to minimize the influence of temperature control on the dynamics.

2.2 Surface Area Analysis

The particle surface area is determined using the MSMS 6.2.1 program[27] which calculates the surface areas of overlapping spheres (here, corresponding to Ti or O ions) numerically and analytically. The radius of the probing sphere was 2.25 Å corresponding to that of a N_2 molecule while the radii of the Ti and O ions are their van der Waals radii, 1.96 and 1.52 Å, respectively[28]. This corresponds to the standard measurement of particle surface area by N_2 adsorption[29].

2.3 GPU Acceleration

The simulations have been run on a common graphics card (NVIDIA GeForce GTX 295) and a desktop workstation (Dell Precision T3400, Ubuntu 9.10, CUDA Version 2.3). Some issues between central (CPU) and graphics processing unit (GPU) simulations have to be considered[30], especially for single precision floating point operations to achieve quite good energy conservation[31]. The open source MD code HOOMD-blue 0.8.2[32] was modified to simulate the TiO_2 pairwise potential of Matsui and Akaogi[16]. The original code running on one GPU attains a performance of around 34 CPUs in parallel on a distributed memory cluster for Lennard-Jones liquids with $r_{cut} = 3\sigma$[32]. There, significant computational time was used on updating the neighbor lists of the ions, but here to account for the long range interactions of the TiO_2 force field all ions have been included in the neighbor lists and therefore it was not updated during the simulations. The implemented TiO_2 potentials have been optimized with single precision runtime math operations and benchmarking the code for different block sizes[33]. This resulted in a speedup of 114 compared to LAMMPS[34] on a single CPU on the same machine for sintering of two TiO_2 particles with $d_{p,0} = 3$ nm (2730 ions). The required memory for the real and “ghost” ions limited the sintering simulations to particles with initial diameters between 5 and 6 nm on the utilized GPU chip.

2.4 Characteristic sintering time

The characteristic sintering time, τ, is the time needed for the sinter neck diameter to reach 83 % of the initial primary particle diameter: $l/d_{p,0} = 0.83$[21]. This corresponds to a 67 % reduction of excess surface area over that of a volume-equivalent fully coalesced sphere. This is close to the reduction of excess surface area of $(1 - 1/e) = 63$ % by exponential models[35] with constant τ[36] that are routinely used in process design for nanoparticle synthesis[11].

The characteristic sintering time of Kobata *et al.*[21] is based on a surface diffusion neck growth model[37]:

$$\tau = 7.44 \times 10^{16} d_p^4 T \times \exp\left(\frac{258'000}{RT}\right) \quad (2)$$

where d_p is the primary particle diameter (m) and T the temperature (K). Using this equation, Kobata *et al.*[21] predicted a final primary particle size of 50 nm in reasonable agreement with experimental data. Based on a grain boundary diffusion neck growth model[37], Seto *et al.*[12] proposed also:

$$\tau = 9.75 \times 10^{15} d_p^4 T \times \exp\left(\frac{258'000}{RT}\right) \quad (3)$$

and simulated the evolution of the particle surface area by accounting for the flow field in good agreement with the measured TiO_2 primary particle diameters of TiO_2 aggregates (d_p = 10 – 100 nm) made in hot-wall aerosol reactors at T = 300 – 1673 K.

3. Results and Discussion

3.1 Evolution of nanoparticle surface area by sintering

Figure 1 shows the evolution of the surface area, a, of two TiO_2 nanoparticles ($d_{p,0}$ = 3 nm) normalized by their initial surface area, a_0, during sintering by MD in a microcanonical (NVE) ensemble (constant energy, black line) with a time step of 1 fs and conserved temperature (NVE with velocity rescaling, red line) with a time step of 3 fs at initial T_0 = 1800 K where both simulations result in a similar surface area evolution. The insets in Fig. 1 show the two TiO_2 nanoparticles (Ti: green and O: red) at t = 0, 0.03, 3 and 150 ns along with the predictions of a common phenomenological model[35] (green line) for two characteristic sintering times, $\boldsymbol{\tau}$.

At the beginning (10^{-5} – 10^{-3} ns), the two particles approach each other and slightly rotate to adjust their lattice planes which has also been observed for example for gold nanoparticles by MD[14] and experimentally[38] and might be an indication of an *oriented attachment* mechanism[39] for TiO_2 where highly mobile particles translate and rotate to find energetically favorable contact points. Then their total surface area might even increase slightly by deformation arising by their ion interactions. Shortly after, sintering starts reducing the surface area in three stages[15]: First by about ~6 – 7 % through adhesion and initial neck growth[18] of the two particles at $t = 10^{-3}$ – 0.01 ns. Second the area is reduced by another 1 – 2 % at 0.01 – 1 ns forming rather oval structures where the sinter neck becomes comparable to the particle diameter and, finally the third stage at about 1 – 100 ns, where the a/a_0 decreases slowly by about 10 % to full coalescence by forming a compact, spherical-like particle.

This stage-wise evolution of sintering has been observed also for micron-sized Cu, Ag and UO_2 particles[40], by boundary integral simulations for viscous sintering of amorphous particles[41] and for MD simulation of iron cluster coalescence[42]. It is consistent also with previous MD of TiO_2[18] for two rutile ($d_{p,0}$ = 3 nm) particles (Fig. 1: blue line) at T = 1473 K (NVE) where after the initial peak of surface area by particle deformation, the first stage of adhesion leads to a similar area reduction. This first stage by Koparde and Cummings[18] occurs later than here because their initial particle separation was 1 nm instead of 0.3 nm here.

Figure 1 shows also that the slope of the final sintering stage is comparable to that (solid green line) of the phenomenological model[35] with the characteristic sintering time of equation (2). Early deviations between the two simulations are caused by the surface area loss by contact and adhesion during the first sintering stage that is not accounted for by that model[35] that underpredicts the surface area evolution by over an order of magnitude indicating that the employed sintering rate of equation (2) is too slow.

Figure 2 shows the evolution of the particle temperature for the simulation of Fig. 1 for constant energy integration (NVE, black line) and conserved temperature (red line). The temperature increases by ΔT = 300 K from 10^{-3} to 100 ns by the conversion of excess surface energy to kinetic energy (NVE) whereas it remains around T = 1800 K for the conserved temperature simulation (red line). Although temperature control can influence ion dynamics, there is little difference between the two calculations with respect to particle surface area dynamics (Fig. 1). To compare the present MD data with the literature and address realistic systems where in most cases the excess heat is removed by colliding gas molecules[42], all subsequent simulations are carried out at conserved temperature.

3.2 Sintering mechanism of TiO_2

The ion mobility and the intrinsic mechanism of TiO_2 nanoparticle sintering are elucidated by coloring the Ti and O ions initially on the particle surface yellow and blue, respectively, while the bulk ones, green and red, as in Fig. 1. Figure 3 shows snapshots of these nanoparticle cross-sections at a) $t = 0$, b) 0.03 ns, c) 3 ns, d) 30 ns, e) 100 ns and f) 150 ns. At $t = 0.03$ ns, the particles have formed a sinter neck mostly by adhesion without much ion relocation leading to the rather large area reduction of the first sintering stage (Fig. 1). Later on, close to the end of the second sintering stage ($t = 3$ ns), the sinter neck diameter has been increased mostly by surface ions (yellow and blue) that have moved over the particle surface and found energetically favorable positions that fit the local lattice (surface diffusion, filled arrows) filling the initially concave region between nanoparticles (Fig. 3c). This has led some of the previously bulk ions to emerge to the particle surface (open arrows) where they increase their mobility.

During the last sintering stage ($t = 30$ ns, Fig. 3d), the two particles have transformed into an oval structured particle. The concave region between nanoparticles has been filled completely by initial surface Ti/O ions during sintering by surface diffusion. In addition, the initial surface ions forming a yellow/blue boundary or zone between coalescing particles (Fig. 3b) have moved away into the initially concave region between particles (Fig. 3e), partially contributing to neck growth during sintering by grain boundary diffusion. Most of the Ti/O ions initially in the core of the nanoparticles are still recognizable and these cores have been deformed slightly by plastic flow[43].

Finally at $t = 150$ ns (Fig. 3f), the particles have fully coalesced into a compact, spherical-like structure. The layer of yellow/blue surface ions at the initial outer edges of the 2-nanoparticles has become very thin or even disappeared at some places (filled arrows). In the core of the fully coalesced particle, there are still two regions of only green/red ions indicating that during sintering the core Ti/O ions experience little net movement. The surface ions in-between the original nanoparticles (Fig. 3b) have been “squeezed” out (no yellow Ti there) into the formerly concave space between the initial particles (open arrows). More green/red bulk ions have emerged to the surface (filled arrows) as the initial surface ions (yellow/blue) have diffused towards the neck region. These green/red ions have increased mobility upon reaching the surface and spread all over it and even on top of the neck region. It is worth noting, however, that mostly red (oxygen) ions are there rather than green (titanium) consistent with the higher mobility of O than Ti ions[44].

These results reveal that sintering of TiO_2 nanoparticles is caused mainly by mobile surface ions while bulk ones remain largely in their place. Surface diffusion appears to be the dominant mechanism during TiO_2 sintering at these particle sizes and temperatures, in agreement with literature[21,45,46]. This is not unreasonable given the high mobility of nanoparticle surface ions, a signature property of nanomaterials. It should be noted, however, that part of sintering takes place also by grain boundary diffusion; a mechanism that should become more important with increasing particle size and number of grains especially in compacted nanoparticle structures with limited free surface.

3.3 Influence of initial primary particle diameter and process temperature

Figure 4 shows the evolution of normalized surface area of two particles at 1800 K with initial particle diameter of $d_{p,0} = 2$ (solid line), 2.5 (dashed), 3 (dash-dot), 3.5 (dash-double-dot) and 4 nm (dotted) as average of 4 simulations with different initial ion positions (supplementary Fig. SI2). For $d_{p,0} = 2$ nm (solid line) the surface area drops quickly by rapid coalescence as for two liquid droplets (supplementary Fig. SI1). Increasing the initial particle diameter leads to slower surface area reduction by neck growth (second sintering

stage, Fig. 1) consistent with experimental observations[12]. The final coalescence stage seems to have a similar slope in the logarithmic time for particle diameters, in agreement with analytical models[47]. The characteristic sintering time, τ, is extracted after the excess surface area of the particles (over that of the fully coalesced ones, a_{fc}) has decreased by 67 % (right axis, horizontal line). This corresponds to $a/a_0 = 0.86$ or a sintering neck diameter of 83 % of the initial primary particle diameter[21].

Figure 5 shows these τ (Fig. 4) obtained by MD simulations at a) 1800 K (circles) and b) 1900 K (squares) and 2000 K (triangles) along with that from equation (2) (solid lines) and equation (3) (dashed lines) as function of initial particle diameter $d_{p,0}$ with decreasing line thickness for increasing temperature. For 1800 K and $d_{p,0} < 3.5$ nm (Fig. 5a), the τ calculated here by MD are significantly lower than those predicted by equations (2) and (3). Nevertheless with increasing initial size ($d_{p,0} > 3.5$ nm), the τ by MD asymptotically converge in-between those predicted by equations (2) and (3) that had been developed for larger particles ($d_{p,0} > 10$ nm) confirming that MD nicely reproduces these literature results. Higher temperatures (Fig. 5b) lead to faster sintering and shorter τ, again between those of equations (2) and (3). The dotted lines in Fig. 5 show a nonlinear fit to the MD data[48]:

$$\tau_{MD} = 3.7 \times 10^{16} d_p^4 T \times \exp\left(\frac{258000}{RT}\left(1 - \left(\frac{3.4 \times 10^{-9}}{d_p}\frac{T}{4100}\right)^{3.76}\right)\right) \quad (4)$$

with d_p in (m), T in (K) and R in (J K^{-1} mol^{-1}).

Figure 6 shows the τ (circles) obtained by MD (supplementary Fig. SI3) along with that of equations (2) (solid line) and (3) (dashed line) as function of temperature for $d_{p,0} = 2.5$ nm as well as the prediction of equations (4) (dotted line). The MD results, however, are for these conditions closer to those from equation (3) by Seto *et al.*[12] and the deviation at higher temperatures is attributed to the approaching of the melting point of TiO_2. The MD data in Fig. 6 (symbols) are matched well by equation (4) (dotted line). As the these data were not used to develop equation (4) as in Fig. 5, this indicates that this equation is able to predict the slower sintering rates (increasing τ) for decreasing temperature and could be used in design of processes for synthesis of small TiO_2 nanoparticles. So when equation (4) is used in the common phenomenological model[35] to describe the nanoparticle surface area during sintering with $d_{p,0} = 3$ nm and T=1800 K (Fig. 1: green broken line), this model comes much closer to the final MD predictions even though it does not closely follow the MD-evolution of surface area.

The shorter τ or faster sintering of smaller nanoparticles given by the MD-derived equation (4) is another manifestation of material properties being different in the nanoscale from the corresponding bulk ones. The higher percentage of surface ions in these particles from 10 nm down to 1 nm, is the most likely reason for their increased sintering rates shown in Fig. 5. This is in excellent agreement with Seto *et al.*[12] who had concluded that nanoeffects on sintering must occur for d_p smaller than 10 nm because no deviation was observed for larger particles. The present MD simulations reveal that indeed this happens for $d_p < 4$ nm.

4. Conclusions

Molecular dynamics (MD) simulations elucidate the sintering of small (2 – 4 nm) rutile TiO_2 nanoparticles to complete or full coalescence at 1500 – 2000 K. Ions on the particle surface exhibited higher net displacement than bulk ones revealing that surface diffusion is the dominant sintering mechanism of TiO_2 nanoparticles. Sintering by grain boundary diffusion takes place to a lesser extent but should increase for larger nanoparticles or for

compacted ones that limit the displacement of surface ions. This might explain conflicting literature on the dominance of surface or grain boundary diffusion during TiO_2 sintering.

The sintering rate was determined quantitatively by monitoring the evolution of the surface area of two coalescing particles at various initial sizes. Lower temperatures or larger initial particle diameters led to longer sintering. For the smallest particle diameters, the MD-obtained sintering rates were smaller than that predicted by theory developed for larger particles. An expression for the sintering rate of rutile TiO_2 nanoparticles has been extracted from MD. With increasing particle size and decreasing temperature, this expression converges nicely to the literature ones for sintering of larger particles. This MD-derived sintering rate facilitates the use of fundamentally-based phenomenological models in design of processes for large scale manufacture and processing of nanoparticles[49].

Supplementary Material

Refer to Web version on PubMed Central for supplementary material.

Acknowledgments

Financial support from Swiss National Science Foundation (SNF) Grant # 200021-119946/1 and European Research Council is gratefully acknowledged.

References

(1). Gratzel M. Nature. 2001; 414:338. [PubMed: 11713540]
(2). Formenti M, Juillet F, Meriaudeau P, Teichner SJ, Vergnon P. J. Colloid Interface Sci. 1972; 39:79.
(3). Teleki A, Pratsinis SE, Kalyanasundaram K, Gouma PI. Sensor. Actuat. B-Chem. 2006; 119:683.
(4). Lademann J, Weigmann HJ, Schafer H, Muller G, Sterry W. Skin Pharmacol. Appl. 2000; 13:258.
(5). Yazdi AS, Guarda G, Riteau N, Drexler SK, Tardivel A, Couillin I, Tschopp J. Proc. Natl. Acad. Sci. 2010; 107:19449. [PubMed: 20974980]
(6). Strobel R, Pratsinis SE. J. Mater. Chem. 2007; 17:4743.
(7). Xiong Y, Akhtar MK, Pratsinis SE. J. Aerosol Sci. 1993; 24:301.
(8). Johannessen T, Pratsinis SE, Livbjerg H. Powder Technol. 2001; 118:242.
(9). Xing Y, Rosner DE. J. Nanopart. Res. 1999; 1:277.
(10). Cho K, Biswas P. Aerosol Sci. Technol. 2006; 40:309.
(11). Muhlenweg H, Gutsch A, Schild A, Pratsinis SE. Chem. Eng. Sci. 2002; 57:2305.
(12). Seto T, Shimada M, Okuyama K. Aerosol Sci. Technol. 1995; 23:183.
(13). Zachariah MR, Carrier MJ. J. Aerosol Sci. 1999; 30:1139.
(14). Arcidiacono S, Bieri NR, Poulikakos D, Grigoropoulos CP. Int. J. Multiphas. Flow. 2004; 30:979.
(15). Collins DR, Smith W, Harrison NM, Forester TR. J. Mater. Chem. 1997; 7:2543.
(16). Matsui M, Akaogi M. Mol. Simulat. 1991; 6:239.
(17). Koparde VN, Cummings PT. J. Phys. Chem. B. 2005; 109:24280. [PubMed: 16375425]
(18). Koparde VN, Cummings PT. J. Nanopart. Res. 2008; 10:1169.
(19). Koparde VN, Cummings PT. ACS Nano. 2008; 2:1620. [PubMed: 19206364]
(20). Garland M, Le Grand S, Nickolls J, Anderson J, Hardwick J, Morton S, Phillips E, Yao Z, Volkov V. Micro IEEE. 2008; 28:13.
(21). Kobata A, Kusakabe K, Morooka S. AIChE J. 1991; 37:347.
(22). Collins DR, Smith W, Harrison NM, Forester TR. J. Mater. Chem. 1996; 6:1385.
(23). Bandura AV, Kubicki JD. J. Phys. Chem. B. 2003; 107:11072.
(24). Thomas BS, Marks NA, Begg BD. Phys. Rev. B. 2004; 69:144122.

(25). Hamad S, Catlow CRA, Woodley SM, Lago S, Mejías JA. J. Phys. Chem. B. 2005; 109:15741. [PubMed: 16852997]
(26). Abrahams SC, Bernstein JL. J. Chem. Phys. 1971; 55:3206.
(27). Sanner MF, Olson AJ, Spehner JC. Biopolymers. 1996; 38:305. [PubMed: 8906967]
(28). Bondi A. J. Am. Ceram. Soc. 1964; 68:441.
(29). Brunauer S, Emmett PH, Teller E. J. Am. Ceram. Soc. 1938; 60:309.
(30). Friedrichs MS, Eastman P, Vaidyanathan V, Houston M, Legrand S, Beberg AL, Ensign DL, Bruns CM, Pande VS. J. Comput. Chem. 2009; 30:864. [PubMed: 19191337]
(31). Hess B, Kutzner C, van der Spoel D, Lindahl E. J. Chem. Theory Comput. 2008; 4:435.
(32). Anderson JA, Lorenz CD, Travesset A. J. Comput. Phys. 2008; 227:5342.
(33). CUDA; Version 2.3. Programming Guide. 2009
(34). Plimpton S. J. Comput. Phys. 1995; 117:1.
(35). Koch W, Friedlander SK. J. Colloid Interface Sci. 1990; 140:419.
(36). Xiong Y, Pratsinis SE. J. Aerosol Sci. 1993; 24:283.
(37). Nichols FA, Mullins WW. J. Appl. Phys. 1965; 36:1826.
(38). Iijima S, Ajayan PM. J. Appl. Phys. 1991; 70:5138.
(39). Barnard AS. Rep. Prog. Phys. 2010; 73:086502.
(40). Ashby MF. Acta Metall. 1974; 22:275.
(41). Garabedian RS, Helble JJ. J. Colloid Interf. Sci. 2001; 234:248.
(42). Lümmen N, Kraska T. Phys. Rev. B. 2005; 71:205403.
(43). Frenkel J. J. Phys. (Moscow). 1945; 9:385.
(44). Kingery, WD.; Bowen, HK.; Uhlmann, DR. Introduction to ceramics. 2nd edition. Chapman Wiley; New York, NY: 1976.
(45). Bonevich JE, Marks LD. J. Mater. Res. 1992; 7:1489.
(46). Kusunoki M, Yonemitsu K, Sasaki Y, Kubo Y. J. Am. Ceram. Soc. 1993; 76:763.
(47). Friedlander SK, Wu MK. Phys. Rev. B. 1994; 49:3622.
(48). SAS. The nonlinear analysis for this paper was generated by the SAS software, Version 9.2 of the SAS System. Copyright © 2011 SAS Institute Inc. SAS and all other SAS Institute Inc. product or service names are registered trademarks or trademarks of SAS Institute Inc.; Cary, NC, USA: 2011.
(49). Pratsinis SE. AIChE J. 2010; 56:3028.

Europe PMC Funders Author Manuscripts

Europe PMC Funders Author Manuscripts

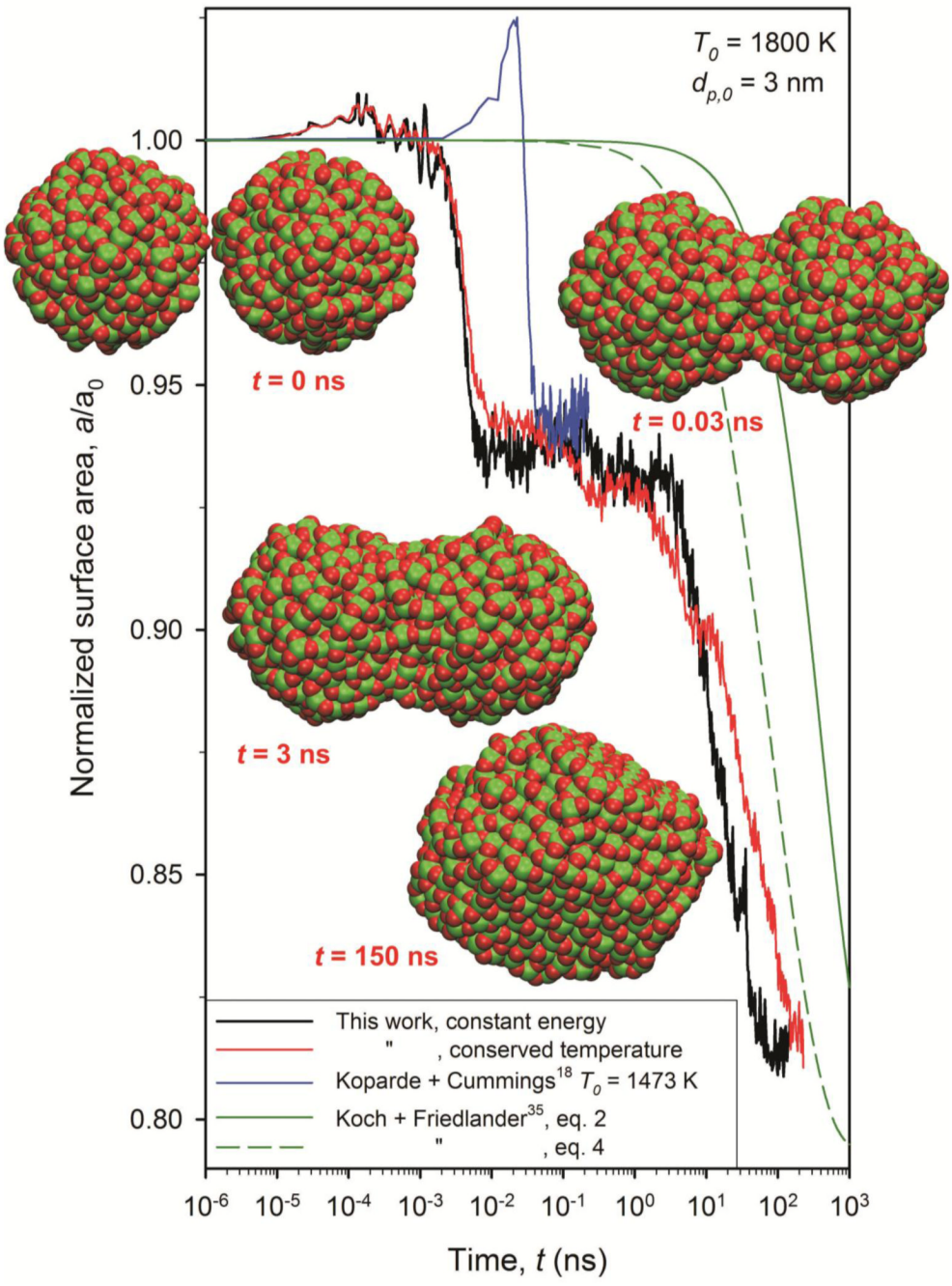

Figure 1.

Evolution of normalized surface area of two sintering TiO_2 nanoparticles ($d_{p,0}$ = 3 nm) by MD for constant energy (black line) and conserved temperature (red line) integration at T_0 = 1800 K along with the MD simulations[18] at 1473 K (blue line, constant energy) and the predictions of a phenomenological model[35] with characteristic sintering times from equation 2 (green solid line) by Kobata *et al.*[21] and equation 4 (green broken line) developed here.

Europe PMC Funders Author Manuscripts

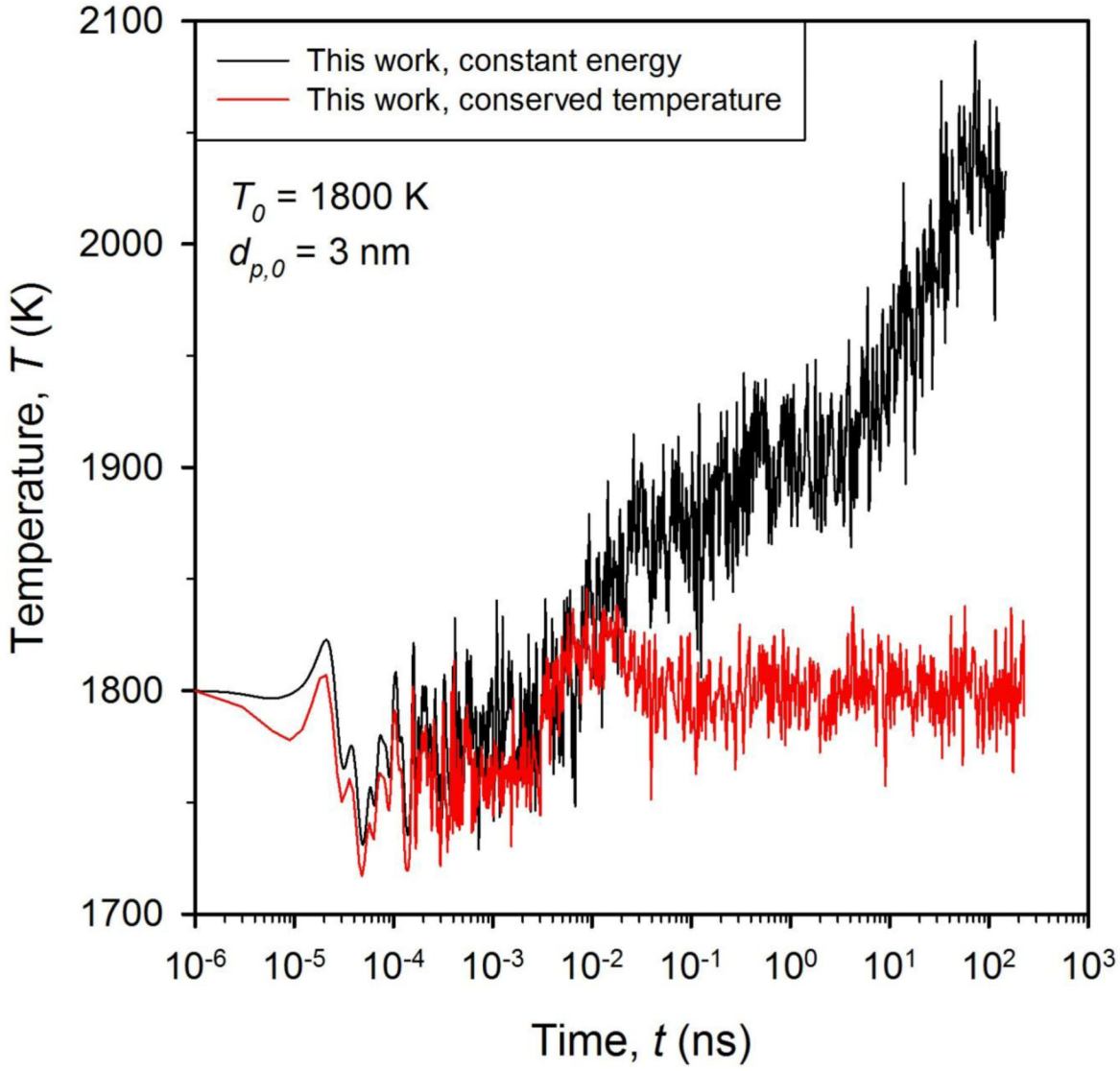

Figure 2.
Evolution of temperature of two sintering TiO_2 nanoparticles ($d_{p,0}$ = 3 nm) for constant energy (black line) and conserved temperature (red line) integration at 1800 K.

Europe PMC Funders Author Manuscripts

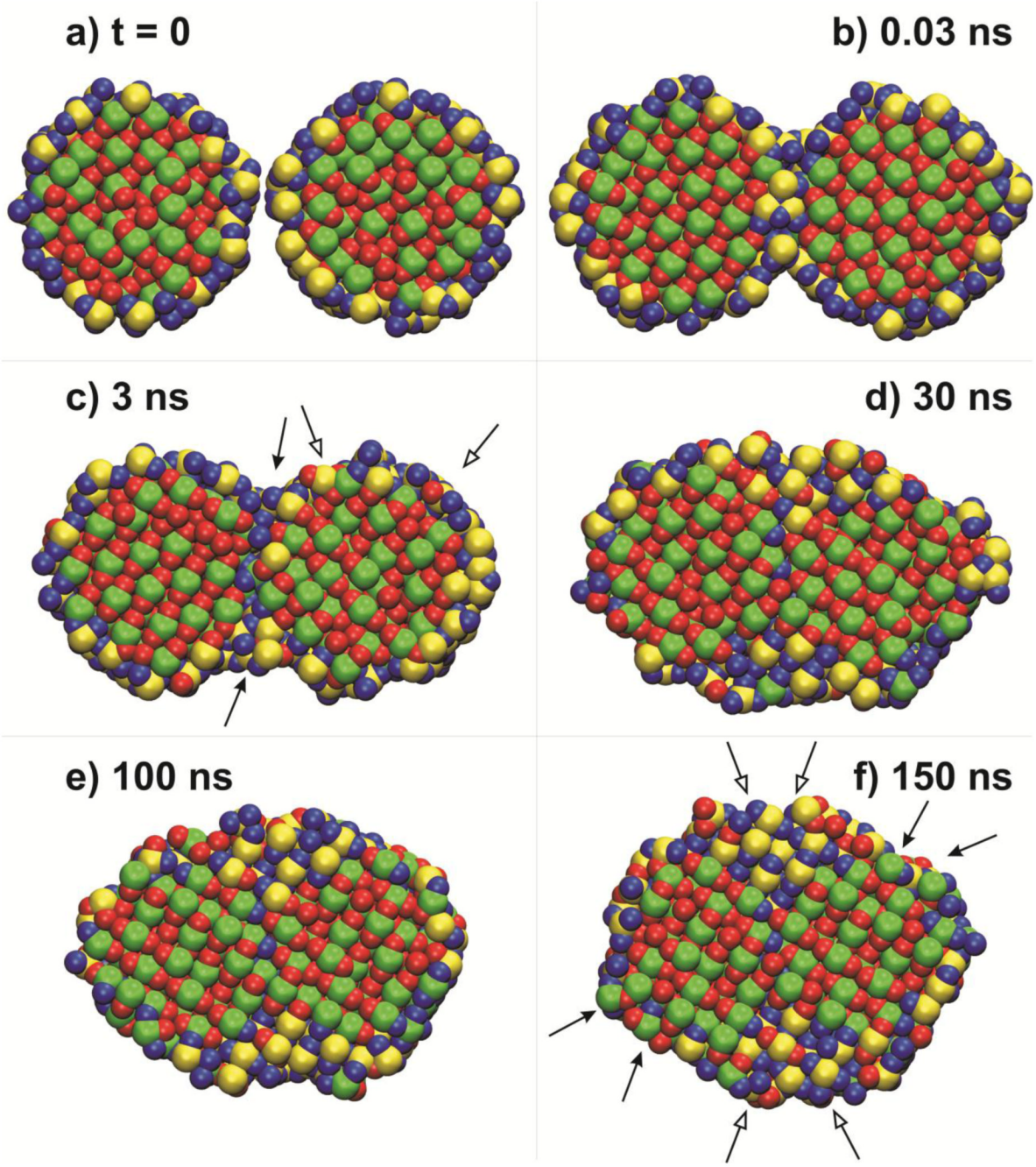

Figure 3.
Snapshots of cross-sections of the particles in Fig. 1 with Ti and O ions initially ($t = 0$ ns) colored green and red (bulk ions) or yellow and blue (surface ions), respectively, at a) $t = 0$, b) 0.03 ns, c) 3 ns, d) 30 ns, e) 100 ns and f)150 ns.

Europe PMC Funders Author Manuscripts

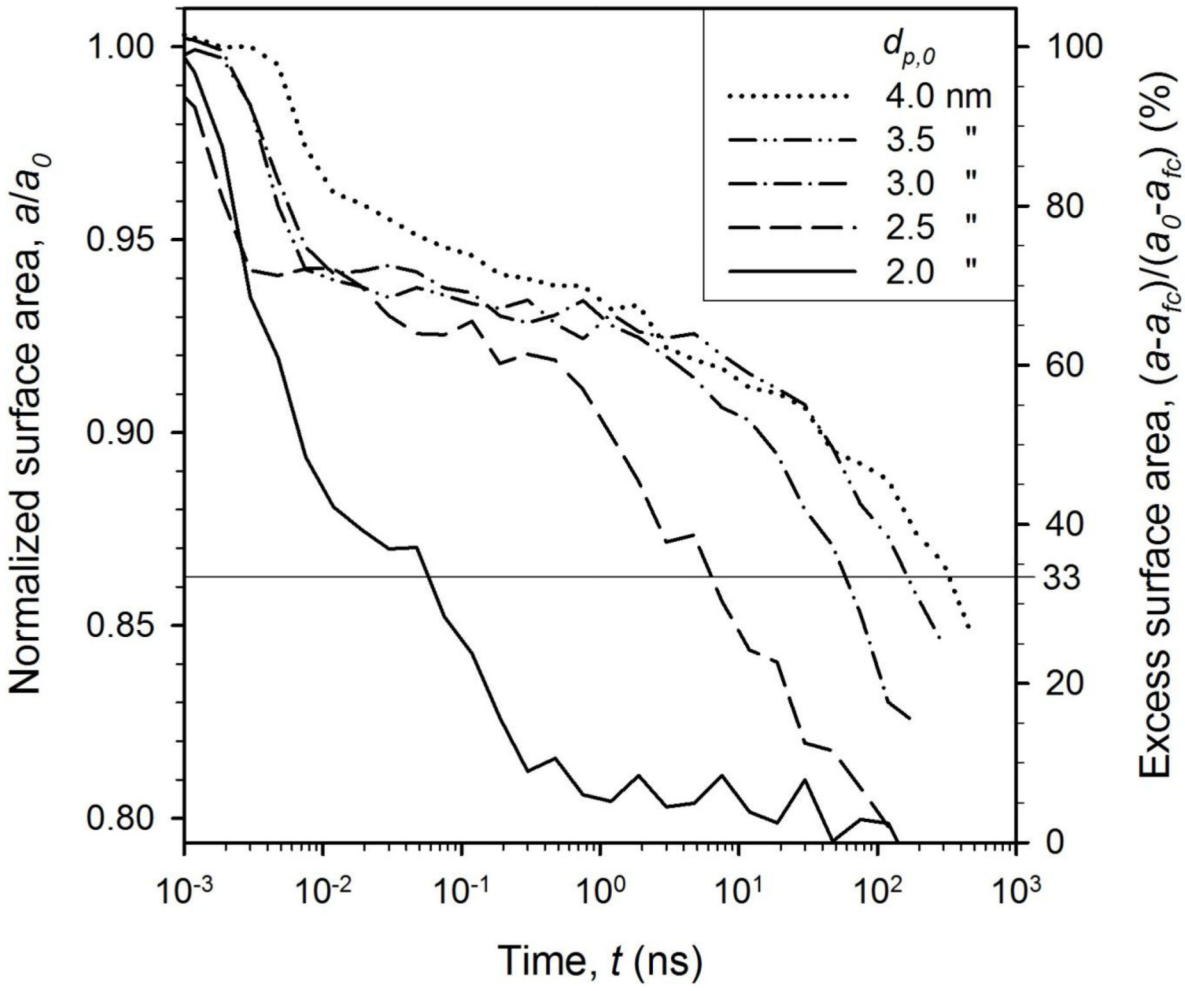

Figure 4.
The evolution of total surface area of equally sized rutile particles with various initial diameters, $d_{p,0}$, at 1800 K. The thin horizontal line where the excess surface area (right axis) has decreased by 67% defines the characteristic sintering time, τ, for each particle size.

Europe PMC Funders Author Manuscripts

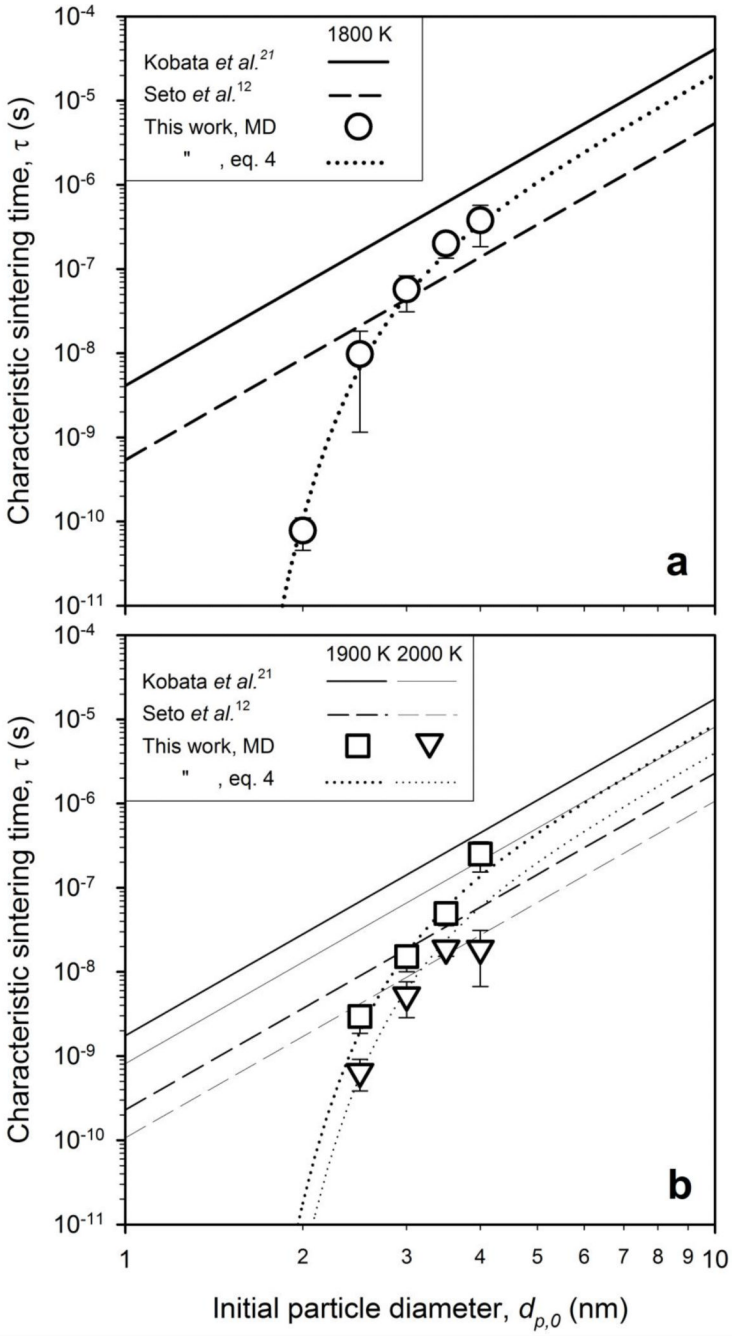

Figure 5.

The characteristic sintering time, τ, obtained from Fig. 4 along with that of Kobata *et al.*[21] (solid lines) and Seto *et al.*[12] (dashed lines) as function of initial primary particle diameter, $d_{p,0}$, at a) T = 1800 K (circles) and b) 1900 K (squares) and 2000 K (triangles). The MD simulations are quantified by equation 4 (dotted line).

Europe PMC Funders Author Manuscripts

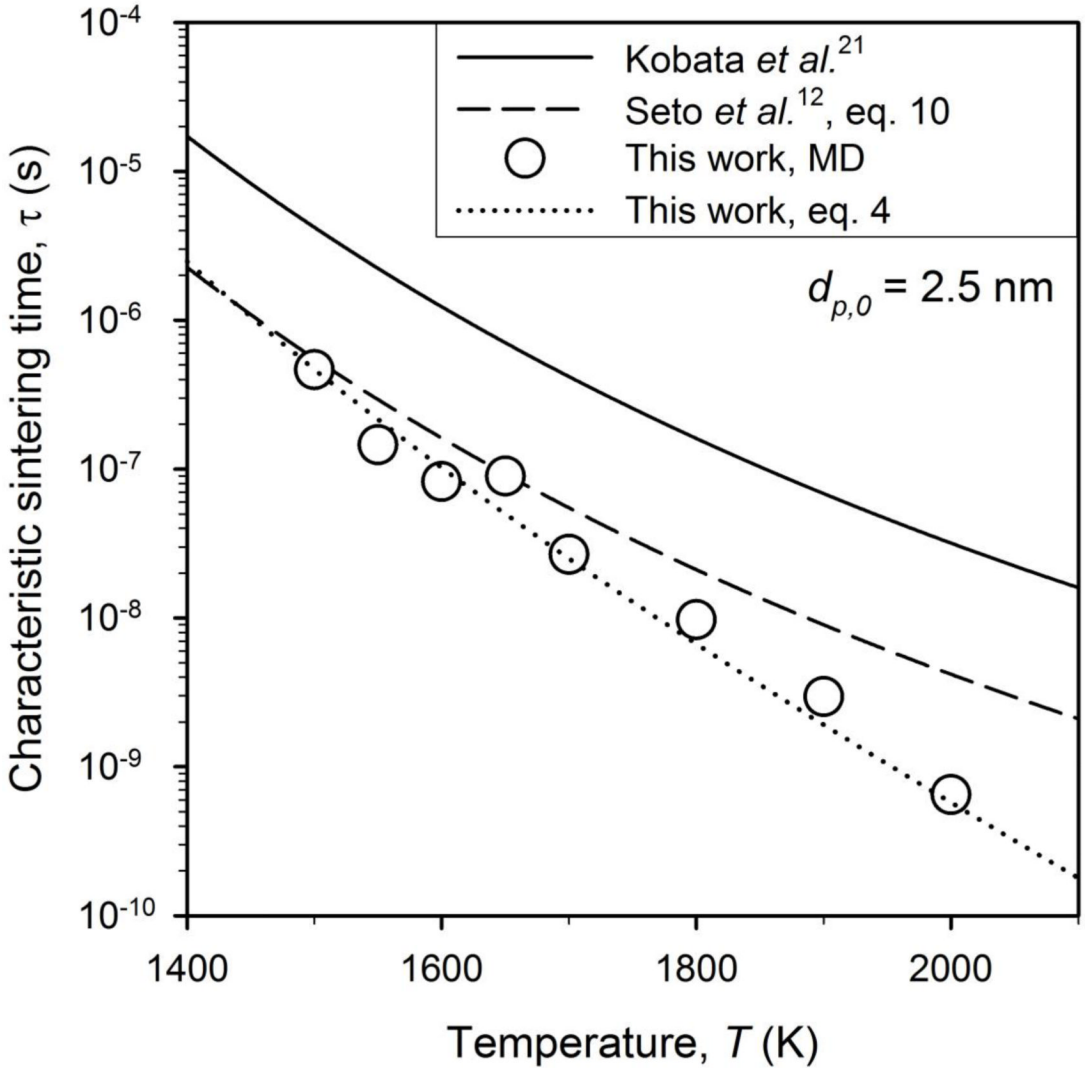

Figure 6.
The characteristic sintering time obtained by the present MD simulations (circles) along with those of equations 2 (solid line), 3 (dashed line) and 4 (dotted line) as function of temperature for $d_{p,0}$ = 2.5 nm. Increasing the temperature leads to shorter characteristic sintering times and therefore faster sintering in agreement with experimental observations.

Europe PMC Funders Author Manuscripts

Table 1

The parameter of the classic pairwise potentials for TiO_2 polymorphs[16]. The constant charges for titanium and oxygen are $q_{Ti} = 2.196$ and $q_O = -1.098$.

ion-ion	A_{ij} [kcal/mol]	B_{ij} [Å]	C_{ij} [kcal Å^6 mol^{-1}]
Ti-Ti	7.177×10^5	0.154	1.210×10^2
Ti-O	3.911×10^5	0.194	2.904×10^2
O-O	2.717×10^5	0.234	6.969×10^2